J. Appl. Comput. Mech., 5(2) (2019) 477-485
DOI: 10.22055/jacm.2018.26819.1360

ISSN: 2383-4536
jacm.scu.ac.ir

M&MoCS
Shahid Chamran University of Ahvaz
Journal of Applied and Computational Mechanics

Research Paper

Hygro-Thermal Nonlinear Analysis of a Functionally Graded Beam

Şeref Doğuşcan Akbaş

Bursa Technical University, Department of Civil Engineering, Yıldırım Campus
16330, Yıldırım/Bursa, Turkey, E-mail: seref.akbas@btu.edu.tr

Received August 20 2018; Revised November 14 2018; Accepted for publication November 19 2018.
Corresponding author: Şeref Doğuşcan Akbaş, seref.akbas@btu.edu.tr

Abstract. Nonlinear behavior of a functionally graded cantilever beam is analyzed under non-uniform hygro-thermal effect. To solve this problem, finite element method is applied within plane solid continua. Total Lagrangian approach is utilized in the nonlinear kinematic relations. Newton-Raphson method with incremental displacement is used in nonlinear solution. Comparison study is performed. Effects of material distribution, temperature and moisture changes on nonlinear deflections of the functionally graded beam are presented and discussed.

Keywords: Functionally Graded Beam; Hygro-Thermal Loading; Nonlinear Analysis; Total Lagrangian Finite Element Method.

1. Introduction

Hgyro-thermal effects or moisture changes have very important role in the mechanics of the structural elements. After a certain moisture value, the structural elements can lost their strength. Functionally graded material (FGMs) is a type of composite in which the properties of materials change directionally. Generally, FGMs are used as thermal barrier systems which produce metal and ceramic materials. As compared to the conventional composite materials, FGMs have more fracture-resistance and structural strength. With the development of technology, FGMs are utilized in many engineering projects such as aircrafts, space vehicles and power plants. Thus, understanding the hgyro-thermal effects on the FGM structures can be very important.

In the last few decades, a lot of investigations have been given to the thermo-mechanical behavior of FGM beams. For example; Rastgo et al. [1] studied instability of FGM curved beams in thermal effects. Li et al. [2] and Song and Li [3] analyzed nonlinear stability of FGM beams under thermal effects. Anadro et al. [4] investigated thermal-postbuckling of FGM beams. Kiani et al. [5] studied thermo-electrical buckling of Timoshenko FGM beams with piezoelectric layers. Fallah and Aghdam [6] examined nonlinear buckling and free vibration of FGM beams resting on nonlinear elastic foundation under thermo-mechanical loading. Kocatürk and Akbaş [7,8], Akbaş and Kocatürk [9] investigated thermal post-buckling of FGM beams by using finite element method. Esfahani et al. [10,11] and Ghiasian et al. [12] analyzed nonlinear thermal stability of FGM beams resting on nonlinear elastic foundation. Zhang and Zhou [13] examined nonlinear and post-buckling responses of FGM beams resting on nonlinear elastic foundation under temperature effects. Akgöz and Civalek [14] studied thermal buckling of FGM micro beams resting on elastic medium. Akbaş [15,16] investigated effects of temperature riding on the dynamic responses of FGM beams. Ebrahimi and Jafari [17],Ebrahimi et al. [18], Akbaş [19,20] studied thermo-mechanical behavior of FGM beams with porosity. Kar and Panda [21] presented nonlinear vibration analysis of FGM panels under thermal loading. Sun et al. [22] studied thermal buckling/post-buckling of FGM beams resting on nonlinear elastic foundation. Dehrouyeh-Semnani [23,24], Dehrouyeh-Semnani et al. [25] investigated nonlinear thermal analysis of FGM beams.

Studies of the porosity effect in the functionally graded structures can briefly classified as follows; Zenkour [26] investigated hygrothermal analysis of exponentially graded rectangular plates. Akbarzadeh et al. [27] analyzed hygrothermal responses of a functionally graded piezoelectric media. Beldjelili et al. [28], Laoufi et al. [29], Boukhelf et al. [30] analyzed

Published online: April 03 2019

hygro-thermal of FGM plates. Mohammadimehr et al. [31] examined static, dynamic and stability of microplate reinforced functionally graded carbon nanotubes under hygro-thermo-mechanical environment. Bakhshizadeh et al. [32] investigated creep analysis FGM rotating thick cylindrical shells under hygro-thermal and magnetic loadings. Barati [33,34], Mouffoki et al. [35], Ebrahimi and Habibi [36], Ebrahimi and Barati [37], Barati and Zenkour [38], Ebrahimi and Barati [39], Hosseini and Kolahchi [40], Jouneghani et al. [41] investigated the hgyro-thermal effects of FGM nano structures. Barati and Shahverdi [42] studied aero-hygro-thermal instability of FGM panels. Nguyen et al. [43] analyzed the dynamic and stability of FGM beams under moisture effects by using the Ritz method.

As can be seen from the literature, nonlinear studies of FGM structures under hygro-thermal loading are not investigated. The novelty in this work consists on nonlinear behavior of a FGM beam under hgyro-thermal. Finite element method with Total Lagrangian two dimensional solid continua is implemented in the modeling and solution of the problem. In nonlinear solution, Newton-Raphson is used with incremental displacement. Effects of material parameter and hgyro-thermal loading on nonlinear deflections of FGM beam are investigated.

2. Theorem and Formulations

A FGM cantilever beam of length L, width b, and height h, under non-uniform temperature and moisture rising is shown in figure 1. ΔT_B, ΔT_T, C_B and C_T stand for temperature rising of bottom surface, temperature rising of top surface, moisture content of the bottom surface and moisture content of the top surface respectively.

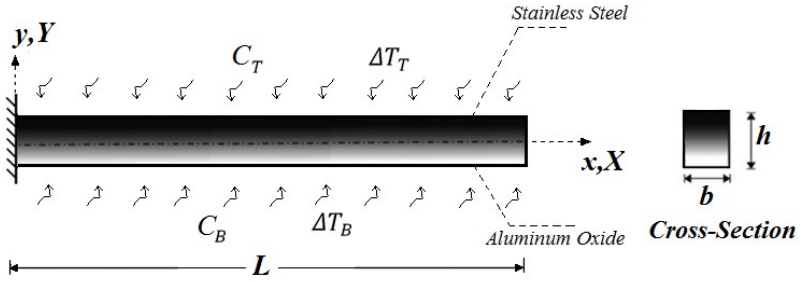

Fig. 1. A cantilever FGM beam under non-uniform moisture and temperature rising.

The material properties, P, change through Y axis based on following power-law function distribution;

$$P(Y)=(P_T-P_B)\left(\frac{Y}{h}+\frac{1}{2}\right)^n+P_B \tag{1}$$

where, P_B and P_T are material properties of bottom and top surfaces, n is the power-law coefficient (material distribution parameter). According to equation (1), when $Y=-h/2$, $P=P_B$, and when $Y=h/2$, $P=P_T$. when $n=0$ material of beam gets homogenous as it is fully from the top material, and when $n=\infty$ material of beam gets homogenous as it is fully from the bottom material. The temperature rise $\Delta T=\Delta T(Y)$ is obtained from heat transfer formulation as follows;

$$-\frac{d}{dY}\left[k(Y)\frac{d\Delta T(Y)}{dY}\right]=0 \tag{2}$$

where, k indicates the coefficient of thermal conductivity. After integration in equation (2), the following expression can be obtained:

$$T(Y)=\Delta T_B+(\Delta T_T-\Delta T_B)\int_{-0.5h}^{y}\frac{1}{k(Y)}dY\Big/\int_{-0.5h}^{0.5h}\frac{1}{k(Y)}dY \tag{3}$$

In hygro-thermal effect, the moisture rising is assumed to nonlinear distribution as a sinusoidal law [43];

$$C(Y)=(C_T-C_B)\left[1-cos\frac{\pi}{2}\left(\frac{2Y+h}{2h}\right)\right]+C_B \tag{4}$$

In the nonlinear kinematic model, total Lagrangian approximation is used within the 2-D solid continuum model by using finite element method. The constitutive formulation with second Piola-Kirchhoff stress and Green-Lagrange strain with hygro-thermal effect is given as:

$${}_0^1S=\begin{Bmatrix}{}_0^1S_{11}\\{}_0^1S_{22}\\{}_0^1S_{12}\end{Bmatrix}=\begin{bmatrix}{}_0C_{11}&{}_0C_{12}&0\\{}_0C_{12}&{}_0C_{22}&0\\0&0&{}_0C_{66}\end{bmatrix}\begin{Bmatrix}{}_0^1E_{11}-\alpha(Y)\Delta T-\beta(Y)\Delta C\\{}_0^1E_{22}\\2\,{}_0^1E_{12}\end{Bmatrix} \tag{5}$$

where ${}_0^1S_{11}$, ${}_0^1S_{22}$, ${}_0^1S_{12}$ is the second Piola-Kirchhoff stress components, ${}_0^1E_{11}$, ${}_0^1E_{22}$ and ${}_0^1E_{12}$ are the Green-Lagrange strain components, ${}_0C_{ij}$ is the reduced constitutive tensor components, α and β are thermal expansion and moisture expansion coefficients, respectively. The reduced constitutive tensor components are given as:

$$ {}_0C_{11} = {}_0C_{22} = \frac{E(Y)}{1-\nu^2(Y)}, {}_0C_{12} = {}_0C_{21} = \frac{\nu(Y)E(Y)}{1-\nu^2(Y)}, {}_0C_{66} = \frac{E(Y)}{2(1+\nu(Y))} \tag{6} $$

where E and ν indicate the Young's modulus and Poisson's ratio, respectively. The Green-Lagrange strain components are stated in as follows;

$$ {}_0^1E = \begin{Bmatrix} {}_0^1E_{11} \\ {}_0^1E_{22} \\ 2\,{}_0^1E_{12} \end{Bmatrix} = \begin{Bmatrix} \dfrac{\partial u}{\partial X} + \dfrac{1}{2}\left[\left(\dfrac{\partial u}{\partial X}\right)^2 + \left(\dfrac{\partial v}{\partial X}\right)^2\right] \\ \dfrac{\partial v}{\partial Y} + \dfrac{1}{2}\left[\left(\dfrac{\partial u}{\partial Y}\right)^2 + \left(\dfrac{\partial v}{\partial Y}\right)^2\right] \\ \dfrac{\partial u}{\partial Y} + \dfrac{\partial v}{\partial X} + \dfrac{1}{2}\left[\dfrac{\partial u}{\partial X}\dfrac{\partial u}{\partial Y} + \dfrac{\partial v}{\partial X}\dfrac{\partial v}{\partial Y}\right] \end{Bmatrix} \tag{7} $$

where u and v indicate displacement components in X and Y directions respectively. Eight-node element plane element is considered in the finite element model as seen from Figure 2.

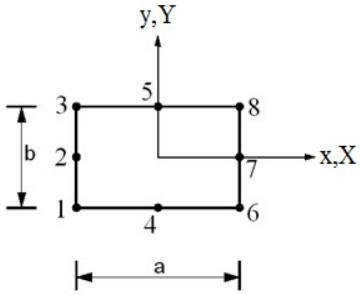

Fig. 2. Eight-node plane element.

Total (δ) and incremental ($\bar{\delta}$) displacements fields are presented following equations:

$$ \{\delta\} = \begin{Bmatrix} u \\ v \end{Bmatrix} = \begin{Bmatrix} \sum_{j=1}^{8} u_j \psi_j(x) \\ \sum_{j=1}^{8} v_j \psi_j(x) \end{Bmatrix} \tag{8} $$

$$ \{\bar{\delta}\} = \begin{Bmatrix} \bar{u} \\ \bar{v} \end{Bmatrix} = \begin{Bmatrix} \sum_{j=1}^{8} \bar{u}_j \psi_j(x) \\ \sum_{j=1}^{8} \bar{v}_j \psi_j(x) \end{Bmatrix} \tag{9} $$

where ψ are the shape functions. The interested reader can find the explicit forms of the shape functions in Akbaş [20]. In i th iteration, finite element equation is given as follows [20]:

$$ \begin{bmatrix} K^{11L} + K^{11NL} & K^{12L} \\ K^{21L} & K^{22L} + K^{22NL} \end{bmatrix}^i \begin{Bmatrix} \bar{u} \\ \bar{v} \end{Bmatrix}^i = \begin{Bmatrix} -F^1 \\ -F^2 \end{Bmatrix}^i \tag{10} $$

where the expressions of $\boldsymbol{K}$ indicate the tangent stiffness matrix, the expressions of $\boldsymbol{F}$ shows the load vector at the i th iteration and $p+1$th load increment. The expressions of $\boldsymbol{K}$ and $\boldsymbol{F}$ are given in below:

$$ \begin{aligned} K_{ij}^{11L} = b\int_A \Bigg\{ & {}_0C_{11}\left(1+\frac{\partial u}{\partial X}\right)^2 \frac{\partial \psi_i}{\partial X}\frac{\partial \psi_j}{\partial X} + {}_0C_{22}\left(\frac{\partial u}{\partial Y}\right)^2 \frac{\partial \psi_i}{\partial Y}\frac{\partial \psi_j}{\partial Y} + {}_0C_{12}\left(1+\frac{\partial u}{\partial X}\right)\left(\frac{\partial \psi_i}{\partial X}\frac{\partial \psi_j}{\partial Y} + \frac{\partial \psi_i}{\partial Y}\frac{\partial \psi_j}{\partial X}\right) + \\ & {}_0C_{66}\left[\left(1+\frac{\partial u}{\partial X}\right)\frac{\partial \psi_i}{\partial Y} + \frac{\partial u}{\partial Y}\frac{\partial \psi_i}{\partial X}\right] \times \left[\left(1+\frac{\partial u}{\partial X}\right)\frac{\partial \psi_j}{\partial Y} + \frac{\partial u}{\partial Y}\frac{\partial \psi_j}{\partial X}\right] \Bigg\} dX\,dY \end{aligned} \tag{11a} $$

$$K_{ij}^{12L}=b\int_A\left\{{}_0C_{11}\left(1+\frac{\partial u}{\partial X}\right)\frac{\partial v}{\partial X}\frac{\partial\psi_i}{\partial X}\frac{\partial\psi_j}{\partial X}+{}_0C_{22}\left(1+\frac{\partial v}{\partial Y}\right)\frac{\partial u}{\partial Y}\frac{\partial\psi_i}{\partial Y}\frac{\partial\psi_j}{\partial Y}+{}_0C_{12}\left[\left(1+\frac{\partial u}{\partial X}\right)\left(1+\frac{\partial v}{\partial Y}\right)\frac{\partial\psi_i}{\partial X}\frac{\partial\psi_j}{\partial Y}+\frac{\partial u}{\partial Y}\frac{\partial v}{\partial X}\frac{\partial\psi_i}{\partial Y}\frac{\partial\psi_j}{\partial X}\right]+ {}_0C_{66}\left[\left(1+\frac{\partial u}{\partial X}\right)\frac{\partial\psi_i}{\partial Y}+\frac{\partial u}{\partial Y}\frac{\partial\psi_j}{\partial X}\right]\times\left[\left(1+\frac{\partial v}{\partial Y}\right)\frac{\partial\psi_j}{\partial Y}+\frac{\partial u}{\partial Y}\frac{\partial\psi_j}{\partial X}\right]\right\}dXdY=K_{ij}^{21L} \tag{11b}$$

$$K_{ij}^{22L}=b\int_A\left\{{}_0C_{11}\left(\frac{\partial v}{\partial X}\right)^2\frac{\partial\psi_i}{\partial X}\frac{\partial\psi_j}{\partial X}+{}_0C_{22}\left(1+\frac{\partial v}{\partial Y}\right)^2\frac{\partial\psi_i}{\partial Y}\frac{\partial\psi_j}{\partial Y}+{}_0C_{12}\left(1+\frac{\partial v}{\partial Y}\right)\frac{\partial v}{\partial X}\left(\frac{\partial\psi_i}{\partial X}\frac{\partial\psi_j}{\partial X}+\frac{\partial\psi_i}{\partial Y}\frac{\partial\psi_j}{\partial X}\right)+ {}_0C_{66}\left[\left(1+\frac{\partial v}{\partial Y}\right)\frac{\partial\psi_i}{\partial X}+\frac{\partial v}{\partial X}\frac{\partial\psi_j}{\partial Y}\right]\times\left[\left(1+\frac{\partial v}{\partial Y}\right)\frac{\partial\psi_j}{\partial X}+\frac{\partial v}{\partial X}\frac{\partial\psi_j}{\partial Y}\right]\right\}dXdY \tag{11c}$$

$$K_{ij}^{11NL}=K_{ij}^{22NL}=b\int_A\left\{{}_0^1S_{11}\frac{\partial\psi_i}{\partial X}\frac{\partial\psi_j}{\partial X}+{}_0^1S_{12}\left(\frac{\partial\psi_i}{\partial Y}\frac{\partial\psi_j}{\partial X}+\frac{\partial\psi_i}{\partial X}\frac{\partial\psi_j}{\partial Y}\right)+{}_0^1S_{22}\frac{\partial\psi_i}{\partial Y}\frac{\partial\psi_j}{\partial Y}^2\right\}dXdY \tag{11d}$$

$$F^1=b\int_A\left\{{}_0^1S_{11}\left(1+\frac{\partial u}{\partial X}\right)\frac{\partial\psi_i}{\partial X}+{}_0^1S_{22}\frac{\partial u}{\partial Y}\frac{\partial\psi_i}{\partial Y}+{}_0^1S_{12}\left[\left(1+\frac{\partial u}{\partial X}\right)\frac{\partial\psi_i}{\partial Y}+\frac{\partial u}{\partial Y}\frac{\partial\psi_i}{\partial Y}\right]\right\}dXdY \tag{11e}$$

$$F^2=b\int_A\left\{{}_0^1S_{11}\frac{\partial v}{\partial X}\frac{\partial\psi_i}{\partial X}+{}_0^1S_{22}\left(1+\frac{\partial v}{\partial Y}\right)\frac{\partial\psi_i}{\partial Y}+{}_0^1S_{12}\left[\left(1+\frac{\partial v}{\partial Y}\right)\frac{\partial\psi_i}{\partial X}+\frac{\partial v}{\partial X}\frac{\partial\psi_i}{\partial Y}\right]\right\}dXdY \tag{11f}$$

In the solution of the nonlinear finite element with total Lagrangian formulations, the small-step incremental method is used. In the iteration steps, the temperature rising is divided by large numbers. The iteration tolerance criterion is used Euclidean norm as given in equation 12. The iteration process is stopped until the difference between last two displacements is more than the tolerance criterion.

$$\sqrt{\frac{\left[\left(d\delta_p^{i+1}-d\delta_p^i\right)^T\left(d\delta_p^{i+1}-d\delta_p^i\right)\right]^2}{\left[\left(d\delta_p^{i+1}\right)^T\left(d\delta_p^{i+1}\right)\right]^2}}\le\zeta_{tol} \tag{12}$$

where

$$\delta_{p+1}^{i+1}=\delta_{p+1}^i+d\delta_{p+1}^i=\delta_p+\Delta\delta_p^i \tag{13}$$

$$\Delta\delta_p^i=\sum_{k=1}^{i}d\delta_p^k \tag{14}$$

3. Results and Discussion

In numerical results, nonlinear deflections of the cantilever FGM beam are calculated for different material distributed-parameter, temperature rising values and moisture rising values. In the numerical examples, the materials of FGM beam are selected as Aluminum Oxide (E=349 GPa, ν=0.26, α=6.86x10^{-6}, k=0.26, β=0.01 *wt %$^{-1}$*) at the bottom surface and Stainless Steel (E=201 GPa, ν=0.3262, α=12.30x10^{-6}, k=15.37, β=0.005 *wt %$^{-1}$*) at the top surface [44,45]. In numerical simulation, the initial temperature is selected as T_0=300 Kelvin (*K*). The geometry of the beam are chosen as: b = 0.2 m, h = 0.2 m, L = 4 m.

It is noted that a non-uniform temperature rising is considered in the numerical study. The temperature increasing of the bottom surface ΔT_B is changed and the temperature of the top surface ΔT_T is constant $\Delta T_T=20K$ in the numerical calculations. Similarly, the moisture content of the bottom surface C_B is changed and moisture content of the top surface C_T is constant $C_T=\%0\,wt$ in the numerical calculations. Hence, the hygro-thermal rising only increases at bottom surface of the FGM beam.

In order to verify this study, the results obtained from this study are compared with those acquired by using ANSYS Workbench 14 [46] which a finite element analysis program presented in table 1. In the comparison study, the nonlinear deflections of free end of beam are calculated for the values of $\Delta T_B=50K, 200K, 400K, 500K$, $\Delta T_T=20K$, $C_T=\%0\,wt$, $C_B=\%0\,wt$ n=0. The beam is modeled as 2D solid continua in ANSYS. As seen from the comparison study in table 1,

results of present report are very close to those of ANSYS Workbench 14.

Table 1. Comparison study: Nonlinear deflections of the free end of beam for different temperature values for n=0.

ΔT_B	u_{max} (Horizontal displacement)		v_{max} (Vertical displacement)	
	Present	ANSYS Workbench 14 [46]	Present	ANSYS Workbench 14 [46]
50 K	0.00172 m	0.00176 m	0.0156 m	0.00165 m
200 K	0.00425 m	0.00431 m	0.1047 m	0.1102 m
400 K	0.00212 m	0.00218 m	0.2516 m	0.2595 m
500 K	0.00263 m	0.00272 m	0.3368 m	0.3420 m

In another comparison study, some results of Jouneghani et al. [41] are compared with obtained results of present report. In the study of Jouneghani et al. [41], static deflections of a simply-supported FGM nano beam are acquired with hygro-thermal and porosity effects based on first shear beam theory and Eringen's nonlocal theory by using Navier method. In the comparison study of table 2, the dimensionless central deflections of FGM beam are presented and compared in results of Jouneghani et al. [41] without nonlocal and porosity effects. Table 2 presents dimensionless central deflections of FGM nano beam with different values of moisture, temperature and material distribution parameter (n). In study of Jouneghani et al. [41], the geometry and material parameters of FGM beam are as follows; L=10 nm, b=h=1 nm, top and bottom surfaces, Ti-6Al-4V and ZrO2 are used. Table 2 shows that results of present study are close to the results of Jouneghani et al. [41] .

Table 2. Comparison study: the hygro-thermal dimensionless central deflections of simply-supported FGM nano beam.

ΔC (% wt)	ΔT (°C)	n					
		0.5		1		5	
		Jouneghani et al. [41]	Present	Jouneghani et al. [41]	Present	Jouneghani et al. [41]	Present
0	0	3.34371	3.3492	2.48445	2.4896	1.76579	1.7691
	50	3.33412	3.3401	2.47921	2.4822	1.76333	1.7655
	100	3.32457	3.3286	2.47399	2.4786	1.76088	1.7632
1	0	2.46429	2.4682	1.74001	1.7442	1.10251	1.1051
	50	2.45907	2.4626	1.73744	1.7411	1.10155	1.1032
	100	2.45388	2.4581	1.73487	1.7280	1.10059	1.1025
2	0	1.95105	1.9572	1.33881	1.3421	0.80145	0.8052
	50	1.94778	1.9522	1.33729	1.3401	0.80094	0.8036
	100	1.94452	1.9496	1.33577	1.3395	0.80043	0.8026
10	0	0.73170	0.7382	0.47062	0.4782	0.25166	0.2535
	50	0.73124	0.7356	0.47044	0.4767	0.25161	0.2531
	100	0.73078	0.7325	0.47025	0.4752	0.25156	0.2522

In figure 3, the effect of the moisture content on maximum hgyro-thermal nonlinear vertical deflections (v_{max}) are presented for n=0.6 with the non-uniform temperature rising. As seen from figure 3, increasing the moisture content, nonlinear deflections increase significantly. Nonlinear deflections of FGM beams change significantly with moisture content.

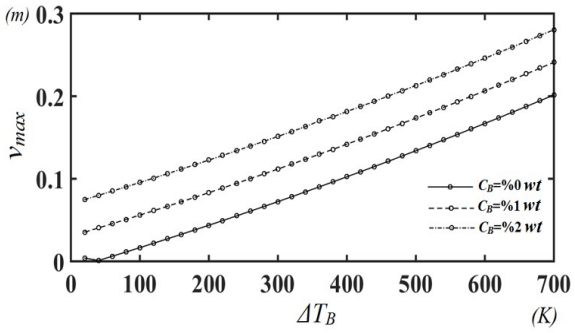

Fig. 3. Temperature rising-maximum vertical displacements (v_{max}) curves for different the moisture content values.

In order to investigate the material distribution parameter on nonlinear displacements of FGM beam, relationship between the moisture content values and the power-law parameter n in the nonlinear deflections of the free end of the beam for different temperature values are shown in table 3 and figure 4. Also, in order to obtain effect of uniform temperature rising, displacement-n relation is depicted for uniform temperature and uniform moisture rising in fig. 4a. Table 3 and figure 4 show that increasing n causes displacements decrease. However, this situation is completely different for the low temperature values and higher moisture content values as seen from fig. 4a and fig. 4b. It is seen from fig. 4a and fig. 4b, the displacements grow with increasing n parameter and moisture in low temperature values. In fig 4a, the bending displacements occur with increasing n value in case uniform temperature and moisture rising. However, the axial displacement occur in case n=0 or ∞. Also, it is seen from table 3 and figure 4 that the difference between among the moisture content values rises with increasing distribution parameter. It shows that power-law parameter is very effective in hgyro-thermal responses of FGM beams.

Table 3. The max. horizontal and vertical displacements of FGM beam for different n, C_B and ΔT_B values.

n	$C_B = \%0\ wt$			$C_B = \%1\ wt$			$C_B = \%3\ wt$		
	$\Delta T_B = 100\,K$	$\Delta T_B = 300\,K$	$\Delta T_B = 700\,K$	$\Delta T_B = 100\,K$	$\Delta T_B = 300\,K$	$\Delta T_B = 700\,K$	$\Delta T_B = 100\,K$	$\Delta T_B = 300\,K$	$\Delta T_B = 700\,K$
0	0.0423 m	0.1742 m	0.5293 m	0.0642 m	0.1951 m	0.5503 m	0.1060 m	0.2369 m	0.5921 m
0.3	0.0260 m	0.1079 m	0.3142 m	0.0595 m	0.1415 m	0.3478 m	0.1266 m	0.2086 m	0.4147 m
0.6	0.0166 m	0.0723 m	0.2015 m	0.0560 m	0.1118 m	0.2409 m	0.1350 m	0.1907 m	0.3199 m
1	0.0113 m	0.0525 m	0.1423 m	0.0541 m	0.0954 m	0.1852 m	0.1398 m	0.1812 m	0.2711 m
3	0.0146 m	0.0620 m	0.1625 m	0.0589 m	0.1063 m	0.2070 m	0.1474 m	0.1952 m	0.2961 m
10	0.0230 m	0.0874 m	0.2264 m	0.0652 m	0.1297 m	0.2689 m	0.1496 m	0.2144 m	0.3538 m

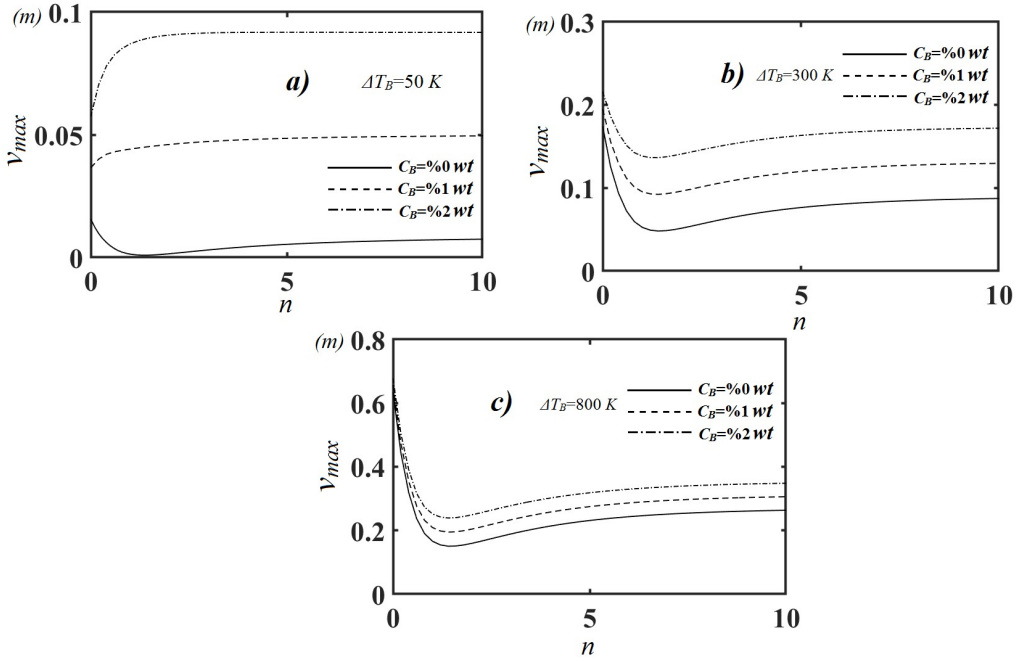

Fig. 4. The relationship between of the moisture content values and the power-law parameter n in the nonlinear displacements for a) $\Delta T_B = 20\,K$ b) $\Delta T_B = 50\,K$, c) $\Delta T_B = 300\,K$ and d) $\Delta T_B = 800\,K$.

Figure 5 displays effect of moisture content values on nonlinear hgyro-thermal deflected shape of the FGM beam for n=0.6 for different temperature values. It is observed from figure 5, there is considerably difference among moisture content values in deflected shape. With increasing moisture content, the nonlinear displacements of FGM beam increase significantly.

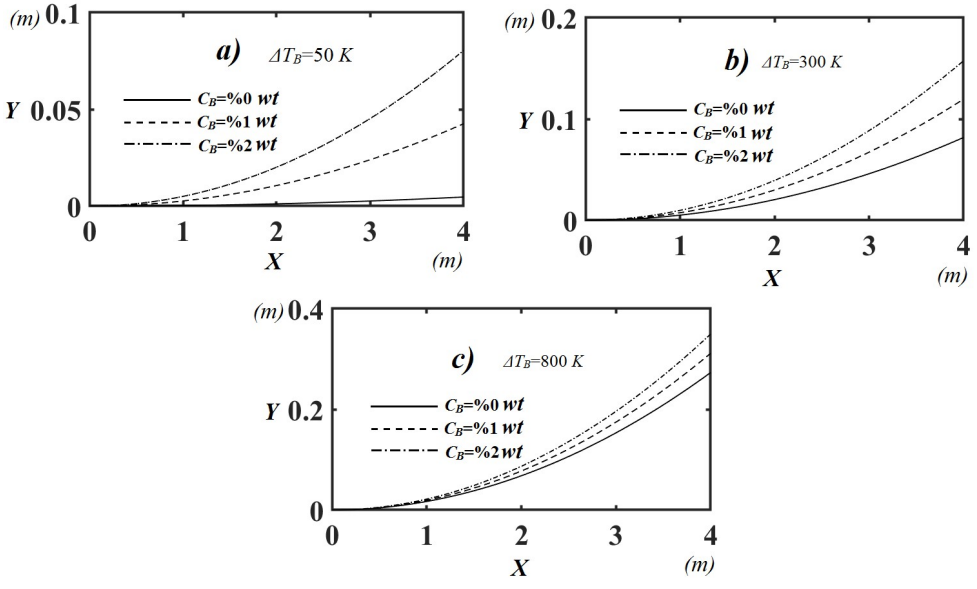

Fig. 5. Effect of the moisture content values on hgyro-thermal nonlinear deflected shape of FGM beam for different temperature values for a) $\Delta T_B = 50\,K$, b) $\Delta T_B = 300\,K$ and c) $\Delta T_B = 800\,K$.

It can also be told from figures 3, 4 and 5 that the difference between the moisture content values in the bending behavior of FGM beams decrease proportionally in higher temperature values. However, this difference is completely different in smaller temperature values. In smaller temperature values, the moisture is more effective than the temperature effect in the bending displacements of FGM beams. As the temperature increases, the effects of moisture on the bending behavior of FGM beams decrease significantly. It shows that the temperature has an important role on the effects of moisture in bending behavior of FGM beams.

Figure 6 displays the effect of n on nonlinear hgyro-thermal displacement shape of the FGM beam when $\Delta T_B = 500\,K$ for different moisture content values. It is observed from figure 6 that n parameter play important role on nonlinear deflections of the FGM beam. As the parameter n increases, the nonlinear deflections of the FG beam decrease considerably. Also, the beam material becomes homogeneous Aluminum Oxide (bottom surface material). The Young modulus of the Aluminum Oxide is larger than Stainless Steel's. Hence, increasing the n yields to higher rigidity and elasticity modulus of the beam.

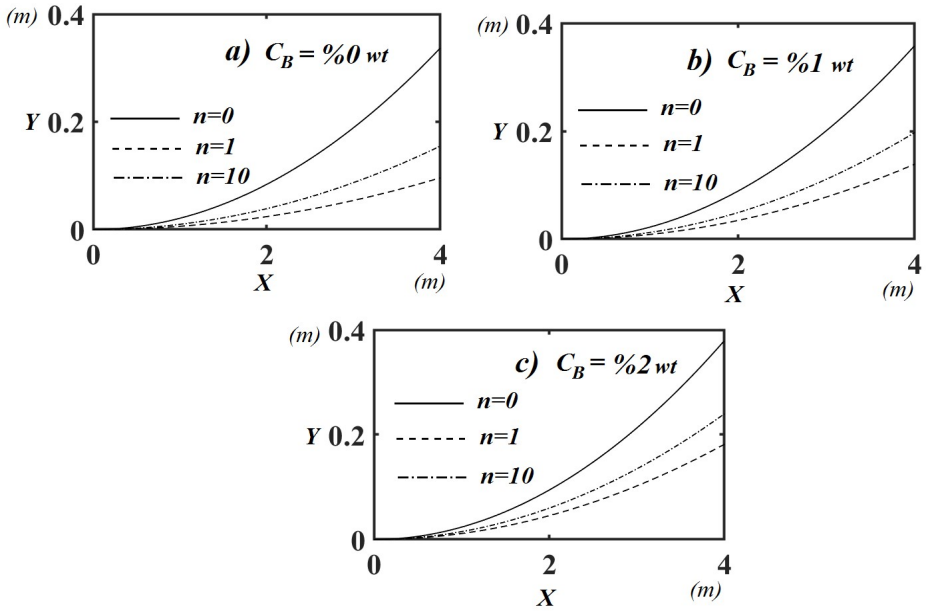

Fig. 6. The relationship between of the moisture content values and the n in the hgyro-thermal nonlinear deflected shape for a) $C_B = \%\,0wt$, b) $C_B = \%\,1wt$ and c) $C_B = \%\,2wt$.

4. Conclusions

Nonlinear Hygro-thermal analysis of a FGM cantilever beam is investigated in this paper. To solve the problem, t he finite element within total Lagrangian 2D continua method is used. In the finite element model of FGM beam, 2D solid is used with Eight-node plane elements. Newton-Raphson is used with incremental displacement is used for the nonlinear solution. Effects of material distribution, temperature and moisture changes on nonlinear deflections of FGM beam are investigated. As seen from the results material distribution and moisture content have important role on the hgyro-thermal responses of the FGM beams. Moisture is very effective in the hgyro-thermal responses of FGM beams. The temperature has an important role on effects of moisture in bending behavior of FGM beams.

Conflict of Interest

The author(s) declared no potential conflicts of interest with respect to the research, authorship and publication of this article.

Funding

The author(s) received no financial support for the research, authorship and publication of this article.

References

[1] Rastgoo A., Shafie H. and Allahverdizadeh A., Instability of curved beams made of functionally graded material under thermal loading, *International Journal of Mechanics and Materials in Design* 2 (2005) 117–128.
[2] Li S.-R., Zhang J.-H., Zhao Y.-G., Thermal Post-Buckling of Functionally Graded Material Timoshenko Beams, Applied *Mathematics and Mechanics (English Edition)* 26(6) (2006) 803-810.
[3] Song X. and Li S., Nonlinear stability of fixed-fixed FGM arches subjected to mechanical and thermal loads, *Advanced Materials Research* 33-37 (2008) 699-706.
[4] Anandrao K.S., Gupta R.K., Ramchandran P. and Rao V., Thermal post-buckling analysis of uniform slender functionally

graded material beams, *Structural Engineering and Mechanics* 36(5) (2010) 545-560.
[5] Kiani, Y., Rezaei, M., Taheri, S. and Eslami, M.R., Thermo-electrical buckling of piezoelectric functionally graded material Timoshenko beams, *International Journal of Mechanics and Materials in Design* 7(3) (2011) 185-197.
[6] Fallah, A. and Aghdam, M.M., Thermo-mechanical buckling and nonlinear free vibration analysis of functionally graded beams on nonlinear elastic foundation, *Composites Part B: Engineering* 43(3) (2012) 1523-1530.
[7] Kocatürk, T. and Akbas, Ş.D., Post-buckling analysis of Timoshenko beams made of functionally graded material under thermal loading, *Structural Engineering and Mechanics* 41(6) (2012) 775-789.
[8] Kocatürk, T. and Akbas, Ş.D., Thermal post-buckling analysis of functionally graded beams with temperature-dependent physical properties, *Steel and Composite Structures* 15(5) (2013) 481-505.
[9] Akbaş, Ş.D. and Kocatürk, T., Post-buckling analysis of functionally graded three-dimensional beams under the influence of temperature, *Journal of Thermal Stresses* 36(12) (2013) 1233-1254.
[10] Esfahani, S.E., Kiani, Y. and Eslami, M.R., Non-linear thermal stability analysis of temperature dependent FGM beams supported on non-linear hardening elastic foundations, *International Journal of Mechanical Sciences* 69 (2013) 10-20.
[11] Esfahani, S.E., Kiani, Y., Komijani, M. and Eslami, M.R., Vibration of a temperature-dependent thermally pre/postbuckled FGM beam over a nonlinear hardening elastic foundation, *Journal of Applied Mechanics* 81(1) (2014) 011004.
[12] Ghiasian, S.E., Kiani, Y. and Eslami, M.R., Dynamic buckling of suddenly heated or compressed FGM beams resting on nonlinear elastic foundation, *Composite structures* 106 (2013) 225-234.
[13] Zhang D.G. and Zhou H.-M., Nonlinear bending and thermal post-buckling analysis of FGM beams resting on nonlinear elastic foundations, *CMES Comput. Modell. Eng.* 100(3) (2014) 201-222.
[14] Akgöz, B. and Civalek, Ö., Thermo-mechanical buckling behavior of functionally graded microbeams embedded in elastic medium, *International Journal of Engineering Science* 85 (2014) 90-104.
[15] Akbaş, Ş.D., Free vibration of axially functionally graded beams in thermal environment, *International Journal Of Engineering & Applied Sciences* 6(3) (2014) 37-51.
[16] Akbas, Ş.D., Wave propagation of a functionally graded beam in thermal environments, *Steel and Composite Structures* 19(6) (2015) 1421-1447.
[17] Ebrahimi F. and Jafari A., A Higher-Order Thermomechanical Vibration Analysis of Temperature-Dependent FGM Beams with Porosities, *Journal of Engineering*, 2016 (2016), 20 p.
[18] Ebrahimi F. Ghasemi F. and Salari E., Investigating thermal effects on vibration behavior of temperature-dependent compositionally graded Euler beams with porosities, *Meccanica* 51(1) (2016) 223-249.
[19] Akbaş, Ş.D., Thermal effects on the vibration of functionally graded deep beams with porosity, *International Journal of Applied Mechanics* 9(5) (2017) 1750076.
[20] Akbaş, Ş.D., Nonlinear static analysis of functionally graded porous beams under thermal effect, *Coupled Systems Mechanics* 6(4) (2017) 399-415.
[21] Kar V.R. and Panda S.K., Geometrical nonlinear free vibration analysis of FGM spherical panel under nonlinear thermal loading with TD and TID properties, *Journal of Thermal Stresses* 39(8) (2016) 942-959.
[22] Sun Y., Li S.-R. and Batra R.C., Thermal buckling and post-buckling of FGM Timoshenko beams on nonlinear elastic foundation, *Journal of Thermal Stresses* 39(1) (2016) 11-26.
[23] Dehrouyeh-Semnani, A.M., On the thermally induced non-linear response of functionally graded beams, *International Journal of Engineering Science* 125 (2018) 53-74.
[24] Dehrouyeh-Semnani, A.M., On boundary conditions for thermally loaded FG beams, *International Journal of Engineering Science* 119 (2017) 109-127.
[25] Dehrouyeh-Semnani, A.M., Mostafaei, H., Dehrouyeh, M. and Nikkhah-Bahrami, M., Thermal pre-and post-snap-through buckling of a geometrically imperfect doubly-clamped microbeam made of temperature-dependent functionally graded materials, *Composite Structures* 170 (2017) 122-134.
[26] Zenkour, A., Hygrothermal analysis of exponentially graded rectangular plates, *Journal of Mechanics of Materials and Structures* 7(7) (2013) 687-700.
[27] Akbarzadeh, A.H. and Chen, Z.T., Hygrothermal stresses in one-dimensional functionally graded piezoelectric media in constant magnetic field, *Composite Structures* 97 (2013) 317-331.
[28] Beldjelili, Y., Tounsi, A. and Mahmoud, S.R., Hygro-thermo-mechanical bending of S-FGM plates resting on variable elastic foundations using a four-variable trigonometric plate theory, *Smart Structures and Systems* 18(4) (2016) 755-786.
[29] Laoufi, I., Ameur, M., Zidi, M., Bedia, E.A.A. and Bousahla, A.A., Mechanical and hygrothermal behaviour of functionally graded plates using a hyperbolic shear deformation theory, *Steel and Composite Structures* 20(4) (2016) 889-911.
[30] Boukhelf, F., Bouiadjra, M.B., Bouremana, M. and Tounsi, A., Hygro-thermo-mechanical bending analysis of FGM plates using a new HSDT, *Smart Structures and Systems* 21(1) (2018) 75-97.
[31] Mohammadimehr, M., Salemi, M. and Navi, B.R., Bending, buckling, and free vibration analysis of MSGT microcomposite Reddy plate reinforced by FG-SWCNTs with temperature-dependent material properties under hgyro-thermo-mechanical loadings using DQM, *Composite Structures* 138 (2016) 361-380.
[32] Bakhshizadeh, A., Zamani Nejad, M. and Davoudi Kashkoli, M., Time-Dependent Hygro-Thermal Creep Analysis of Pressurized FGM Rotating Thick Cylindrical Shells Subjected to Uniform Magnetic Field, *Journal of Solid Mechanics* 9(3) (2017) 663-679.
[33] Barati, M.R., Investigating dynamic response of porous inhomogeneous nanobeams on hybrid Kerr foundation under hygro-thermal loading, *Applied Physics A* 123(5) (2017) 332.

[34] Barati, M.R., Vibration analysis of FG nanoplates with nanovoids on viscoelastic substrate under hygro-thermo-mechanical loading using nonlocal strain gradient theory, *Structural Engineering and Mechanics* 64(6) (2017) 683-693.
[35] Mouffoki, A., Bedia, E.A., Houari, M.S.A., Tounsi, A. and Mahmoud, S.R., Vibration analysis of nonlocal advanced nanobeams in hygro-thermal environment using a new two-unknown trigonometric shear deformation beam theory, *Smart Structures and Systems* 20(3) (2017) 369-383.
[36] Ebrahimi, F. and Habibi, S., Nonlinear eccentric low-velocity impact response of a polymer-carbon nanotube-fiber multiscale nanocomposite plate resting on elastic foundations in hygrothermal environments, *Mechanics of Advanced Materials and Structures* 25(5) (2018) 425-438.
[37] Ebrahimi, F. and Barati, M.R., Effect of three-parameter viscoelastic medium on vibration behavior of temperature-dependent non-homogeneous viscoelastic nanobeams in a hygro-thermal environment, *Mechanics of Advanced Materials and Structures* 25(5) (2018) 361-374.
[38] Barati, M.R. and Zenkour, A., Forced vibration of sinusoidal FG nanobeams resting on hybrid Kerr foundation in hygro-thermal environments, *Mechanics of Advanced Materials and Structures* 25(8) (2018) 669-680.
[39] Ebrahimi, F. and Barati, M.R., A modified nonlocal couple stress-based beam model for vibration analysis of higher-order FG nanobeams, *Mechanics of Advanced Materials and Structures* 25(13) (2018) 1121-1132.
[40] Hosseini, H. and Kolahchi, R., Seismic response of functionally graded-carbon nanotubes-reinforced submerged viscoelastic cylindrical shell in hygrothermal environment, *Physica E: Low-dimensional Systems and Nanostructures* 102 (2018) 101-109.
[41] Jouneghani, F.Z., Dimitri, R. and Tornabene, F., Structural response of porous FG nanobeams under hygro-thermo-mechanical loadings, *Composites Part B: Engineering* 152 (2018) 71-78.
[42] Barati, M.R. and Shahverdi, H., Aero-hygro-thermal stability analysis of higher-order refined supersonic FGM panels with even and uneven porosity distributions, *Journal of Fluids and Structures* 73 (2017) 125-136.
[43] Nguyen, T.K., Nguyen, B.D., Vo, TP. and Thai, H.T., Hygro-thermal effects on vibration and thermal buckling behaviours of functionally graded beams, *Composite Structures* 176 (2017) 1050-1060.
[44] Reddy J.N. and Chin C.D., Thermoelastical Analysis of Functionally Graded Cylinders and Plates, *Journal of Thermal Stresses* 21(6) (1998) 593–626.
[45] Sobhy, M., An accurate shear deformation theory for vibration and buckling of FGM sandwich plates in hygrothermal environment, *International Journal of Mechanical Sciences* 110 (2011) 62-77.
[46] ANSYS Workbench Release 14.0, SAS IP, Inc, 2012.